Lignocellulosic plant cell wall variation influences the structure and properties of hard carbon derived from sorghum biomass

Rana Arslan Afzal[a], Jordan Pennells[a], Yusuke Yamauchi[a,b], Pratheep K. Annamalai[b,*], Ashok Kumar Nanjundan[a,*], Darren J. Martin[a,*]

[a] School of Chemical Engineering, The University of Queensland, St Lucia, Brisbane 4072, Australia
[b] Australian Institute for Bioengineering and Nanotechnology, The University of Queensland, St Lucia, Brisbane 4072, Australia

ARTICLE INFO

ABSTRACT

Agricultural by-products offer attractive renewable feedstock options for the production of carbon to be used as electrode materials for energy storage applications. Developing insights into the carbonisation behaviour of these alternative feedstocks will enable us to tune the materials and processing conditions effectively. For the first time, this study reports the influence of lignocellulosic biomass variation on the structure and properties of sorghum-derived hard carbon materials. Four primary plant sections of sorghum biomass (leaf, sheath, upper stem and bottom stem), with different lignocellulosic composition and hierarchical native plant cell wall morphology, were partitioned from the harvested biomass and subsequently carbonised. Thermal and structural analysis of these sections before and after carbonisation revealed that both the morphology and associated lignocellulosic composition were influential upon the structure and properties of the resultant carbon. The leaf section with the highest lignin and ash content yielded 23% carbon, with high crystallinity and a higher existence of graphite-like domains. It also exhibited a highly porous structure and a large specific surface area. The sheath section with the highest cellulose content yielded 26% carbon with thinner graphitic layers and a larger D-spacing compared to other sections. Stem sections with high extractives facilitated early-stage stabilisation. The upper stem, which had the lowest lignin and ash content, yielded 25% carbon with the lowest BET surface area and pore volume. In contrast, the bottom stem yielded 30% carbon with more disordered turbostratic hard carbon and a lower D-spacing compared to other sections. It is noted that a higher graphitic carbon ratio can be achieved by selecting a biomass precursor with a higher lignin content and lower crystallinity index. Additionally, the value of BET surface area and pore volume strongly correlates with starting lignin content. This research contributes to developing a more sophisticated and comprehensive understanding of how the subtle structural and compositional variations present in different plant sections of sorghum biomass can influence the properties of carbonised materials, hopefully aiding the future potential for enhanced tunability of sustainable biomass-derived carbon products.

Introduction

Carbon is an exceptionally versatile and ubiquitous material used in a myriad of applications. Consequently, the demand for new and improved carbon materials is increasing in the global market. Fossil fuel-derived materials have been the traditional precursors for carbon materials. However, as with many other material platforms, these sources are limited and unsustainable. Lignocellulose biomass is naturally abundant, renewable, and emerging as a sustainable precursor for carbon production [1 7]. Recently, many agricultural residues have been explored as promising sources of lignocellulosic biomass due to their abundance, low initial cost, and fast biomass accumulation [8 13]. Carbon has been prepared from numerous agricultural residues such as stems, shells, stones, fibres, peels, seeds, husks, and other waste [14]. Different biomass precursors generated various types of carbon under the same growth conditions [15]. This is due to the naturally biodiverse and unique features of different plants. According to Deng et al [16]., cellulose, hemicellulose, and lignin have a significant ef-

* Corresponding authors.
E-mail addresses: p.annamalai@uq.edu.au (P.K. Annamalai), ashok.nanjundan@uq.edu.au (A.K. Nanjundan), darren.martin@uq.edu.au (D.J. Martin).

fect on the properties of the resultant carbon material due to their different intrinsic structures. Similarly, each section of a plant has unique hierarchical plant cell wall structures and features due to its specific role in the overall plant structure and physiology. So if processed or refined in the same manner, it is typical to observe a phenomenon where each plant section produces different material products [17]. This has been explored in the context of cellulose nanofibre (CNF) research but has not previously been extended to investigate the effects on carbonised material properties [17 20].

Consequently, the plant section plays a vital role in the resultant material properties [17,19,21,22] and should be considered an essential parameter. However, traditionally the *whole plant* is harvested and used for the pyrolysis of carbon, generally neglecting biomass variation across different plant tissues and therefore potentially overlooking the opportunity to design and tune higher performance, higher value carbon materials that are more "fit-for-purpose". To achieve improved control and obtain the best possible carbon property profile from lignocellulosic precursors, it is therefore essential to understand the carbonisation behaviour of all predominant plant sections separately. This approach should advance our understanding of the relationship between biomass and derived carbon properties to a point where, potentially, we might consider separating agricultural residues into numerous grades of lignocellulose precursors, thus giving rise to specific carbon grades.

Sorghum, an ideal crop for arid or marginal land, is the fifth most grown cereal crop worldwide in grain production [23]. It is an attractive modern commercial crop, in part due to its high drought tolerance and capacity to limit transpiration under high evaporative demand, small upper leaves, and deep rooting behaviour [24]. It has high biomass production for biofuel and livestock feed applications [25,26]. It can grow well in traditionally less-favourable farming areas and has an impressive pedigree of disease resistance. Despite that, the systematic study of sorghum to obtain active carbon is seldom reported [27,28]. In this study, we report the physicochemical properties of systematically partitioned primary plant sections, i.e., leaf, sheath, upper stem and bottom stem of sorghum biomass before and after carbonisation, to understand the influence of lignocellulosic composition and cell morphology on the carbonisation behaviour and to facilitate the development of a more comprehensive structure-property relationship. To the best of our knowledge, no study is available that correlates biomass variation across different plant sections to biomass-derived carbon structure and properties. For this, we have chosen the Sugargraze^{TM} sorghum variety for its biomass quality and yield based on a broader study involving several varieties as part of a more substantial research project [29].

Materials and methods

Materials

The sorghum (Sugargraze^{TM}) biomass was harvested from the University of Queensland's research facility (27°32′45′′S, 152°19′44′′E) at the Gatton campus after three months seeding.

Separation of plant sections

To investigate the different plant sections separately, manual separation of leaf, sheath, and stem was performed in the lab. Further separation of the stem was performed, and the components were separated into two parts: less than 1 metre above ground (bottom stem) and greater than 1 metre above ground (upper stem). The separated sorghum sections were further cut into small pieces (∼5 cm lengths), and any decayed plant material was removed and discarded. The plant sections' percentages in terms

of their wet weight were calculated (Table S1, Supplementary material). Each sorghum section was washed separately thrice for approximately 30 min with plenty of hot distilled water (80 °C) and dried for three days at ∼55 °C in a convection oven. Dried sorghum section materials were ground with an SM 300 Retsch cutting mill (3000 rpm - 1 mm mesh). Samples were dried in a vacuum at 50 °C for 24 h to remove any residual moisture for further use and characterisation.

Lignocellulosic composition

The lignocellulosic composition of ground biomass samples was analysed by a near-infrared spectroscopy (NIRS) method at Celignis Biomass Analysis Laboratories, Limerick (Ireland). This analysis was performed with visible and near-infrared radiation (wavelength: 400–2500 nm). A FOSS XDS monochromator having Rapid Content Analyser (RCA) and Vision 3.5 software was used for this purpose [22].

Carbonisation

Biomass samples were carbonised at 1000 °C under a constant nitrogen flow in a ceramic tube furnace (Carbolite). Carbonisation involved an initial stabilisation by heating up to 240 °C at a heating rate of 5 °C/min and holding for 2 h, followed by stepping up to a maximum carbonisation temperature of 1000 °C at a heating rate of 5 °C/min and again holding for 2 h. The ceramic tube was removed from the furnace upon cooling to room temperature, and the carbon product was weighed and stored.

Thermal gravimetric analysis

To investigate the thermal stability and carbonisation yield of lignocellulose, thermal gravimetric analysis (TGA) and derivative thermogravimetric (DTG) analysis were performed. The analysis was done using a thermogravimetric analyser (TGA STARe System, Metler Toledo) by heating the samples from 25 °C to 500 °C at a rate of 5 °C/min, under a flow of nitrogen.

X-ray diffractometer

Bruker D8 Advance X-ray diffractometer (Bruker, Germany) was used to perform X-ray diffraction (XRD) analysis with a Cu Kα source (λ=1.54 Å) at 45 kV and 40 mA. The scanning rate was 1° per minute or 1.2 s per step with the range of 5 to 60°. The value of full width at half maximum (FWHM) was found after fitting the peak using a Gaussian curve. The crystallinity Index (CrI) was evaluated from XRD diffraction patterns by using the following relation proposed by Segal et al [30].:

CrI $= (I_{200}\text{-}I_{amp}/I_{200})$x100 where I$_{200}$ is the intensity of the (200) peak and I$_{amp}$ is the hump between peaks (200) and (110) ($2\theta = 18°$) [30,31].

The interlayer spacing (d_{002}) of biomass-derived carbon samples was calculated using the Bragg's law equation: d$_{002}$ = $\lambda/2sin\Theta$ where λ is the wavelength of Cu Kα radiation (0.154 nm), Θ is the diffraction angle [32].

The thickness of graphite-like structure L$_c$ of biomass-derived carbon samples is calculated by:

Lc=$k\lambda/\beta sin\Theta$ where λ is the wavelength of Cu Ka radiation, then $K = 0.89$, β is FWHM of (002) peak [32].

The average number of graphene layers of biomass-derived carbon was calculated by:

N=L$_c$/d$_{002}$

The average length L$_a$ of the graphite-like structure of biomass-derived carbon was calculated by:

L$_a = k\lambda/\beta sin\Theta$

Where β is the FWHM of (100) peak [32].

X-ray photoelectron spectrometry

X-ray Photoelectron Spectrometry (XPS) was used to evaluate the surface composition, using a Kratos Axis ULTRA X-ray Photoelectron Spectrometer incorporating a 165 mm hemispherical electron energy analyser. The incident radiation was Monochromatic Al Kα X-rays (1486.6 eV) at 150 W (15 kV, 10 mA). The vacuum-dried samples were scanned at an analyser pass energy of 160 eV over 1200–0 eV binding energy range with 1.0 eV steps and a dwell time of 100 ms for a wide survey and at 20 eV with 0.05 eV steps and 250 Ms dwell time for narrow high-resolution survey. During sample analysis, the base pressure in the analysis chamber was 10–9 Torr and 10–8 Torr. Atomic concentrations were calculated using the CasaXPS version 2.3.14 software and a Shirley baseline with Kratos library Relative Sensitivity Factors. Samples were run in duplicates, and one spot on each sample was analysed. Peak fitting of the high-resolution data was also performed using the CasaXPS software. All high-resolution scans were charge-corrected to the C−C peak at 284.6 eV.

Scanning electron microscopy

Morphological aspects of plant sections before and after carbonisation were analysed by Scanning electron microscopy (SEM). Additionally, scanning electron microscopy–energy-dispersive X-ray spectrometry (SEM-EDS) analysis was performed to identify the elemental composition of the materials. Before scanning, the samples were coated with a thin platinum layer (about 15 nm). The plant section samples were loaded on the stub placed horizontally for the surface analysis and vertically for the cross-section view with the help of carbon tape. The carbonised sample was dispersed into ethanol by ultrasonic treatment with a treatment duration of 1 min and deposited on the cleaned silicon substrate while drying on a hotplate. The samples were placed on the stub with the help of carbon tape, coated with thin layer platinum ($\sim$15 nm) and scanned using an SEM (JEOL 7001F) operating at 8 kV is used to analyse the derived carbon samples.

Raman microscopy

Carbonised samples were investigated using a Raman spectrophotometer coupled with a microscope (inVia 2, Renishaw) with a laser wavelength of 514 nm. Prior to the scan, calibration was performed using reference silicon materials at Raman active vibration peak (520 cm^{-1}). Raman spectrum of carbonised samples was deconvoluted using a Gaussian fit to calculate A_D (1350 cm^{-1}) and A_G (1590 cm^{-1}) ratio.

Nitrogen adsorption

The Micromeritics® Instrument Corporation TriStar II was used to measure samples' porosity and specific surface area. Nitrogen adsorption/desorption isotherms were measured at – 196 °C. Before measurement, samples were degassed by VacPrep^{TM} 061 at 80 °C for 30 min and then 200 °C for 6 h in a vacuum of 15 psig to eliminate moisture and other volatiles. The Specific surface area and pore volume were calculated by Brunauer-Emmett-Teller (BET) and Non-Linear Density Function Theory (NLDFT) methods.

Attenuated total reflectance fourier transform infrared spectroscopy (ATR-FTIR)

Nicolet 6700 spectrophotometer was used to perform ATR-FTIR analysis. Measurements were taken from 500 to 4000 cm^{-1} in the transmittance mode at 4 cm^{-1} resolution with the accumulation of 32 scans per analysis. The spectrometer uses ATR ImaginG Accessory with a diamond crystal window. Spectrum software facilitates obtaining the spectra.

Results and discussion

The influence of chemical and structural features of plant section on the structure and properties of carbon is discussed by comparing the results before and after carbonisation.

Lignocellulosic composition of plant sections

The "whole-plant" sorghum biomass comprises 10% sheath, 13% leaf, and 73% stem by mass, after 4% grain separation (Table S1, Supplementary material). The stem section is divided into three parts: a tip, upper stem, and bottom stem, which constitute 3, 30 and 40% by mass, respectively. Cellulose, hemicellulose and lignin are the main lignocellulosic components [33] Table 1. presents the lignocellulosic components (i.e., cellulose, hemicellulose, lignin, extractives, and ash) present in the various water-washed plant sections as analysed by the NIRS method. Further details on all compositions can be seen in Table S2 (Supplementary material). Lignocellulosic composition depends on the specific features and functions of plant sections and disease [34,35]. It is noted that the four primary plant sections are associated with slightly different lignocellulosic ratios, and this is due to the presence of an uneven distribution of organic and inorganic compounds during plant development [10].

Lignin covalently links cellulose and hemicellulose and forms a protecting boundary, which provides strong mechanical support to increase the recalcitrance of the lignocellulosic biomass [33]. Lignin consists of many aromatic units has a high carbon content, is chemically inert, thermally stable [16] and facilitates the development of a layered and microporous carbon structure after carbonisation [36]. Similar lignin content is generally present for the Sugargraze^{TM} sorghum variety compared to other agricultural by-products and sorghum varieties. This can be seen in Table S3 (Supplementary material) and in the work reported by N. Reddy et al [17].. Additionally, lignin also provides protection against pests and pathogens [35]. Q. Liu et al [35]. reported that the cell wall of pathogen-infected plants accumulated increased amounts of lignin. This lignin accumulation creates a primary barrier that prevents the spread of disease and reduces fungal and toxin infiltration into plant cell walls [35]. Our results show that the amount of lignin is highest in the leaf and decreased from sheath to bottom stem and upper stem (Table 1). We also observed that the leaves of the sorghum plant were more infected with pathogens than other parts of the plant.

The amount of lignin content in the leaf is 21%. In reported studies, the range of lignin in sorghum leaves varies from 9 to 33% (Table S3, Supplementary material). Additionally, the lignin content in the sorghum upper and the bottom stem is 14 and 17%. In reported studies, the lignin content in stem varies from 6 to 18% (Table S3, Supplementary material). Furthermore, the higher amount of lignin in the bottom part of the stem compared to the upper part is in agreement with another reported sorghum stem study where the lower stem had a more "woody" texture (Table S3, Supplementary material) [21].

Cellulose is the fundamental and structural component of all green plant primary cell walls. This fibrous, resilient, and water-insoluble polysaccharide provides a stable structure and tensile strength to the primary cell wall and fibers [33]. The thermal stability of cellulose is highly dependant on its crystallinity [37]. Due to oxygenated functional groups, cellulose forms a mesoporous structure in carbon upon pyrolytic treatments [36]. During carbonisation, after desorption of physically adsorbed water around 25 to

Table 1

Compositional and crystallinity information for primary sorghum plant sections was obtained by lignocellulosic analysis, XRD (including EDS analysis)~~, mercury porosimeter~~ and XPS.

	Leaf	Sheath	Upper stem	Bottom stem
Cellulose	28	35	24	26
Hemicellulose	17	19	9	9.5
Lignin	21	18	14	17
Extractives	7	4	37	28
Ash	9.5	9	5	5.5
XRD Crl (%)	46	46	41	54
XPS survey analysis[atomic%]	C: 81O: 16N: 2.5Si: 0.7	C: 79O: 18N: 1.2Si: 1.5	C: 69O: 28N: 2.1	C: 72O: 26N: 1.2Sr 0.03
EDS analysis[Wt%]	C: 65O: 14Si: 18Ca: 2	C: 12O: 21Si: 66	C: 81O: 13K: 5	C: 62O: 16Si: 17Cl: 2K: 3

150 °C, splitting-off of structural water occurs from 150 to 240 °C [31,37,38]. Afterwards, chain scissions and depolymerization reactions occur during the range of 240 to 400 °C [31,37,38]. This is proceeded with the breaking of C—O and C—C bonds within ring units, along with the removal of more water, CO, and CO_2. Finally, aromatization and carbonization above 400 °C or the formation of graphite-like layers occurs at elevated temperatures [31,37,38]. It is postulated that the final carbon residue generated from each cellulose ring unit is based on four-carbon atoms, which act as the basic building blocks for graphite layer formation [31,39]. Overall, cellulose content (28%) present in the Sugargraze[TM] sorghum plant lies within the range of published values for other sorghum varieties (21–36%) [40]. Still, it is lower than some of the other agricultural by-products presented in Table S3 (Supplementary material). Again, the reasons for these differences can be broadly ascribed to evolution and mechanical function. A higher cellulose content is noted in those plants which need to support a relatively higher weight of the fruit or grain, for example, pineapple and banana fibers in Table S3 (Supplementary material). On the other hand, fibers of bagasse, corn stover, sorghum stalks, barley, wheat and rice straw have a lower cellulose content and are associated with the relatively smaller weights of grain as compared to pineapple and banana, as shown in Table S3 (Supplementary material) [17,34]. The same concept applies to the plant sections; for example, the sheath is also required to support the relatively higher leaf weight and so is associated with a higher cellulose content. The sheath has the highest amount of cellulose (35%) as compared to other plant sections, namely leaf, bottom stem, and upper stem, as indicated by the fraction of total sugar and ratio of α-cellulose. The sheath is an elongated, cylindrical structure that acts as a protective covering and supports the relatively larger sized leaves of the plant. A higher alpha-cellulose content in the sheath helps the plant to remain stiff and strong. Likewise, the stem being the largest portion of the plant shows slight variations in cellulose content depending on height. In the upper stem and bottom stem, we measured 24 and 26% of cellulose, respectively. These values are near compared to the reported range for stems from other species of sorghum, where they reported 27 to 65% (Table S3, Supplementary material). However, the difference may be attributed to different the methods used to characterise lignocellulose composition within the literature. Additionally, the cellulose content of sorghum (Sugargraze[TM]) sheath and leaf is very similar to the other reported non-wood agricultural by-products like wheat straw, corn stover and rice (30–40%) [17].

Hemicellulose is a combination of typically amorphous polysaccharides present in the plant's secondary cell wall and, together with cellulose, lignin, protein, and other materials, they provide water-binding and viscoelastic properties to the green plant cell wall. Mechanically, hemicellulose has little contribution in terms of fibre strength and stiffness. In comparison with cellulose, hemicellulose has an amorphous structure and low degree of polymerization, therefore lower thermal and chemical stability and is consequently easily degradable into monosaccharides [41]. Overall, the

sorghum plant studied here appears to have a lower hemicellulose content than other sorghum varieties [40] and other reported agricultural waste (Table S3, Supplementary material). The hemicellulose content is lower in the upper stem and higher in the sheath. The hemicellulose content decreases from sheath > leaf > bottom stem > upper stem.

Extractives are the non-structural components of lignocellulosic biomass. They are elements that tend to resist insect attack and decay by fungi. Upper stems have the highest extractives. Extractives typically have low thermal stability and provide early-stage stabilisation during carbonisation.

Components that contribute to residual ash, such as silica (SiO_2) phytoliths present in grasses, facilitate functional protective features against plant-feeding organisms, help retain outer structure, and additionally stop the plant from wilting during drought. The ash content is higher in sorghum (Sugargraze[TM]) than other reported sorghum varieties [17], presumably associated with drought tolerance traits [10]. Research shows that a high amount of ash is linked with low micropore surface area [42]. However, it is also reported that biomass precursors with high ash content generate porous materials [43,44].

The influence of these compositional variations is perhaps more well-understood in the pulp and paper and biofuels industries. Fibres with higher cellulose contents have better properties and are relatively easier to process (refine or fibrillate). This is because noncellulosic components such as lignin make it more difficult to bleach the fibres, and lignin also makes the fibres stiff, harsh to handle [17,19] and "recalcitrant" in terms of subsequent mechanical or chemical biorefining [45 48]. In the well-established micro and nanocellulose fibre literature, a higher amount of hemicellulose and a lower amount of lignin certainly facilitate the use of milder chemicals (delignification and bleaching, for example) and less energy-intensive mechanical fibrillation treatments [49 51]. On the other hand, the influence of lignocellulosic composition on carbonation behaviour is not as well understood. This work investigates this behaviour by systematically investigating sorghum plant sections and their subsequent carbonisation. The sorghum upper stem section was associated with the lowest lignin content within the plant. Therefore, this upper stem material is likely more amenable to further pulping and mechanical refining than the bottom stem.

X-ray diffraction (XRD) analysis

X-ray diffraction (XRD) analysis was performed to understand the influence of lignocellulosic composition on the hard carbon formation as a function of the degree of crystallinity. The X-ray diffractograms of water washed sorghum leaf, sheath, upper stem and bottom stem are presented in Fig. 1a. The XRD patterns displayed a combination of crystalline peaks with a broad, amorphous hump centred at around 18.5 2θ. Well-defined crystalline cellulose I peaks can be seen at 2θ around 15°, 16°, 22°, and 34°, which correspond to (101), (10Ī), (200), and (004) planes, respectively
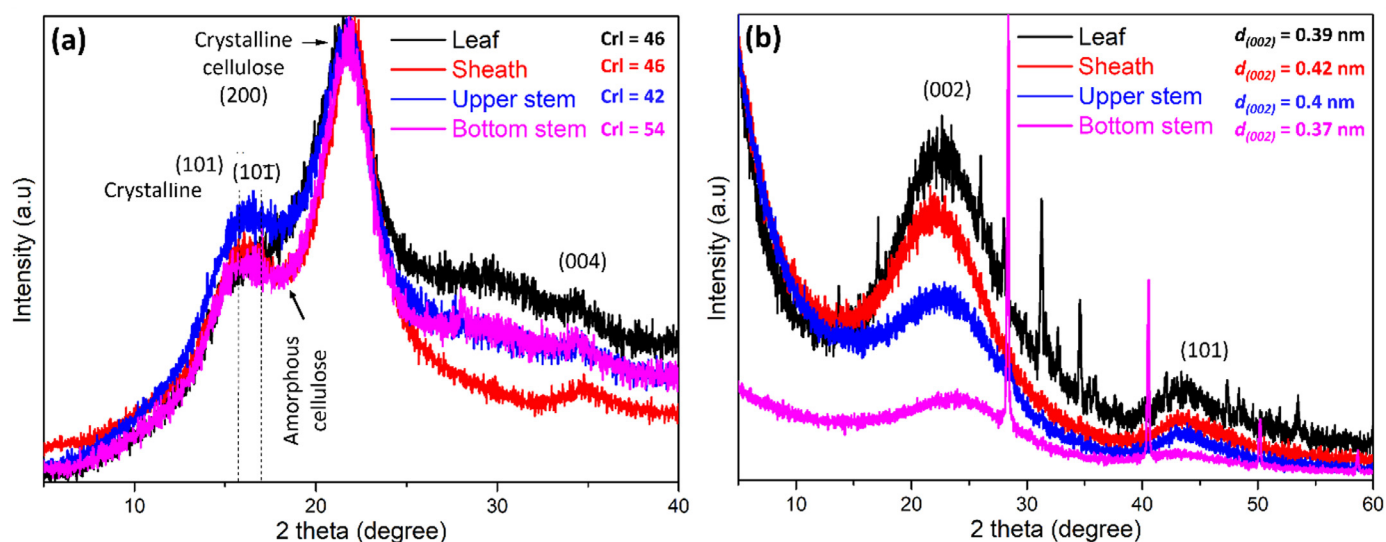
Fig. 1. XRD pattern of water-washed sorghum plant sections (leaf, sheath, upper and bottom stem); (a) before and, (b) after carbonisation at 1000 °C.

[31,37]. The hump around 18.5° is associated with the amorphous phase or disordered regions. The Crystallinity Index (CrI) is a measure of the degree of cellulose order within the biomass. The intensity of the amorphous phase is lower in the bottom stem section, suggesting less amorphous components, and corroborated by the higher CrI. The calculated CrI of sorghum leaf, sheath, upper and bottom stem were 46, 46, 41 and 54%, respectively. The amorphous, hemicellulose-rich regions facilitate water channelling and other chemical absorptions for the sorghum plant cell wall. Sorghum plant section fibres have a relatively low CrI compared to the reported percentage crystallinity values for corn husk, cotton, corn stalks, and linen fibres [17]. In fact, the percentage CrI of the sorghum plant section fibres is lower than most other reported lignocellulosic fibres [17] but falls within the range of other reported sorghum varieties (31–50%) [52]. Generally, the percentage crystallinity of fibres could be associated with the growth habit and breeding of the commercial crop varieties. Sugargraze™ Sorghum is bred primarily as a forage cultivar for animal feed. As such, it is relatively easy to grow and promotes more plant and less grain (i.e., zero or very small seed heads). Therefore, it could be argued that these commercially bred plants may inherently have a lower crystallinity simply because of these requirements of less mechanical integrity (to support large, heavy seed heads) and fast growth requirements [17,19,28].

After the carbonisation of sorghum at 1000 °C, the diffraction peaks at (101), (10Ī), (200), and (004) disappear. The two broad peaks around at $2\theta = 21°$ and 43.8° assigned to the (002) and (101) reflections of turbostratic carbon are now observed [20,53]. The XRD patterns for the four carbonised sorghum plant sections are shown in Fig. 1b. The prominent sharp peaks can be seen for the leaf and bottom stem sections, corresponding to various common inorganic deposits. Quartz phytoliths (Q) are commonly present in grass leaves [54]. Calcite I improves leaf photosynthesis for a plant grown under water deficit (sorghum is an arid grass species) [55]. The familiar presence of inorganic deposits also depends on the growth conditions. As discussed above, leaf sections have higher ash than other parts of plants.

Furthermore, the bottom stem section is the lower part of the plant stem, closer to the soil. The (002) peak of the leaf is narrower and slightly more intense than the others, revealing a higher graphitisation degree. We suggest that this is primarily due to the higher lignin content [16,31,56]. The more robust thermal stability of aromatic units in lignin makes it more stable. It is presented in

Table 2 that leaf, sheath, upper stem, and bottom stem section derived carbons are associated with the graphite-like nanocrystal interlayer spacing (d_{002}) of 0.39, 0.42, 0.4 and 0.37 nm, respectively. The minimum D-spacing obtained is more than 0.335 nm, which is close to the interlayer spacing of graphite [57]. The obtained graphite-like nanocrystal domains are further investigated by the average thickness (L_c), length (L_a) and the number of graphene layers (N) [32]. The number of graphene layers (N) has a high influence on the properties of graphene-based materials and their applications. The optical absorption and electrical resistance of graphene are proportional to the number of graphene layers. The higher number of layers reflects more incident light in the visible region. Similarly, the electrical resistance increases when the number of layers decreases [58]. For hard carbon anodes, a higher graphitisation degree can be associated with a lower charge transfer resistance [16]. It is usually believed that the number of layers of graphene is dependant on their production method [58], but in this work, it is noted that it is also dependant on the unique features of the biomass precursors (Table 1 and 2).

Raman spectroscopy

The Raman spectra of carbonised sorghum plant sections are shown in Fig. 2. The G peaks in 1580 cm^{-1} represent the vibrations of sp^2-carbon atoms in the ring and chain structure, i.e., ordered carbon. D peaks in 1350 cm^{-1} represent the vibrations of sp^3-carbon atoms, i.e., disordered carbon. The high intensity of G peaks is noted in all carbonised samples of sorghum plant parts, which indicates a high graphitisation degree [20,53]. The D-band and G-band peaks were deconvoluted using Gaussian fit and the D/G ratio (A_D/A_G) was calculated using the area under the curve Table 2. presents the A_D/A_G ratio for leaf, sheath, upper and bottom stem. The calculated A_D/A_G ratio for carbonised leaf is 2.2, which is lower than carbonised sheath (2.7), upper stem (2.5) and bottom stem (2.8). A lower D/G ratio of carbonised leaves suggests a higher proportion of ordered carbon.

The D/G ratio is influenced by lignin content (thermally stable aromatic units) [16] and CrI [31,56] Fig. 3. shows the correlation of the A_D/A_G ratio with lignin content and biomass CrI. Leaf and sheath have the same CrI. Leaf has higher lignin content than the sheath, which co-occurs with lower disordered carbon content. Leaf has a higher CrI and lignin value than upper stem. The difference of lignin content is higher than the difference of CrI, so

Table 2
Structural properties of sorghum sections carbonised at 1000 °C, as obtained by different analytical techniques.

	Leaf	Sheath	Upper stem	Bottom stem
d_{002} (nm)	0.39	0.42	0.4	0.37
L_a (nm)	4.2	3	4	2.7
L_c (nm)	3.9	3.1	3.2	4.2
N	10	7.5	7.9	11
A_D/A_G	2.2	2.7	2.5	2.8
S_{BET} (m²/g)	311	197	54	71
Pore volume (cm³/g)	0.22	0.13	0.03	0.04
XPS survey analysis [atomic%]	C: 82O: 14Si: 4	C: 76O: 18Si: 5Na: 0.6	C: 92O: 7.4Si: 0.6	C: 91O: 8Cl: 0.9
EDS analysis[Wt%]	C: 78O: 3Si: 3Mg: 3P: 4Ca: 7	C: 84O: 13Si: 0.7Mg: 0.2P: 0.3K: 0.9	C: 84O: 12Si: 1Mg: 0.3P: 0.2K: 2	C: 85O: 2Si: 2Cl: 7Cl: 1K: 3
Yield% at 500 °C (TGA) at 1000 °C (Manual)	2723	2526	25 25	3028

d_{002} is Interlayer spacing calculated at (002) by Bragg's law.
L_a and L_c is the average length and thickness of the graphite-like structure, respectively.
N is an average number of graphene layers.
A_G and A_D are the area of the G band and D band in Raman.
S_{BET} is BET surface area.
Yield% at 500 °C from TGA and at 1000 °C by manual calculation.
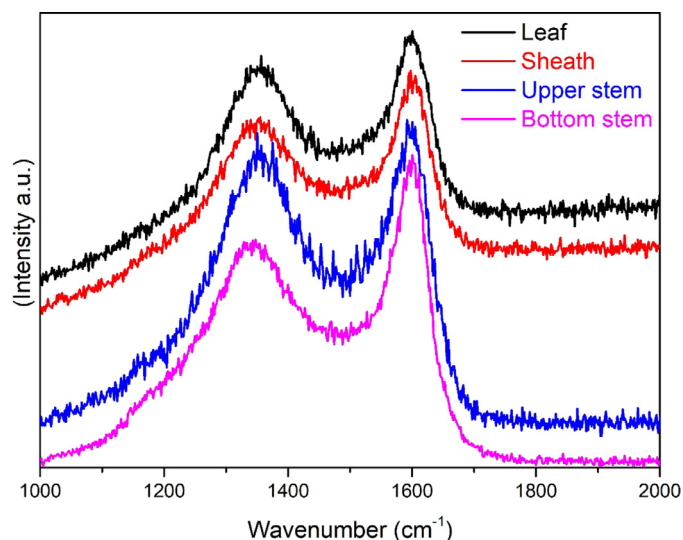
Fig. 2. Raman spectra of carbonised sorghum plant sections.
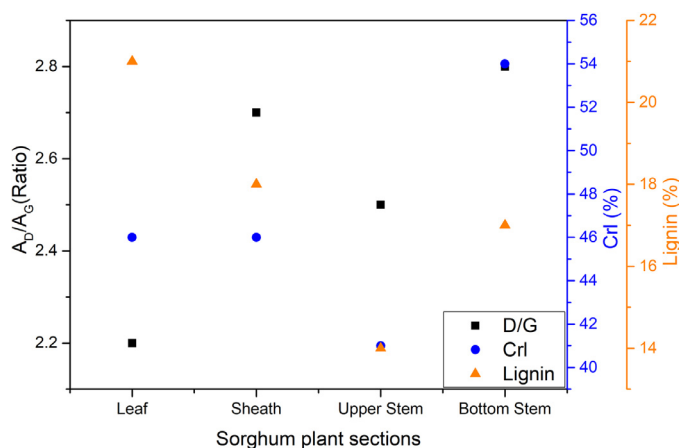
Fig. 3. Lignin content and Crl value of the plant sections and their potential influence on the A_D/A_G ratio in Raman spectra of carbonised samples.

the impact of lignin is more prominent than Crl and more disordered carbon is produced in the upper stem than the leaf. The sheath has a higher Crl and lignin value than the upper stem as well, but the difference of Crl is higher than the difference of lignin content, so the impact of Crl is more prominent than lignin, and less disordered carbon is produced in the upper stem as compared to the sheath. Leaf and sheath both have higher lignin and lower Crl than the bottom stem and have lower disordered carbon than the bottom stem. The upper stem has a lower lignin value than the bottom stem, but the very high Crl value of the bottom stem contributes more heavily than the lignin influence and ultimately leads to a more disordered carbon. Hence, lignocellulosic composition and structural features of precursor can significantly influence the properties of the derived carbon.

Morphological characterisation

SEM images were taken to compare the native morphological differences between the four plant sections. Water-washed sorghum sections surface and cross-section SEM images are shown in Fig. 4. The sorghum water-washed leaf surface displays multiple open pores or stoma (Fig. 4a), facilitating photosynthesis. Additionally, the other elongated structures on the leaf surface can be associated with trichomes [59]. The leaf cross-sectional view
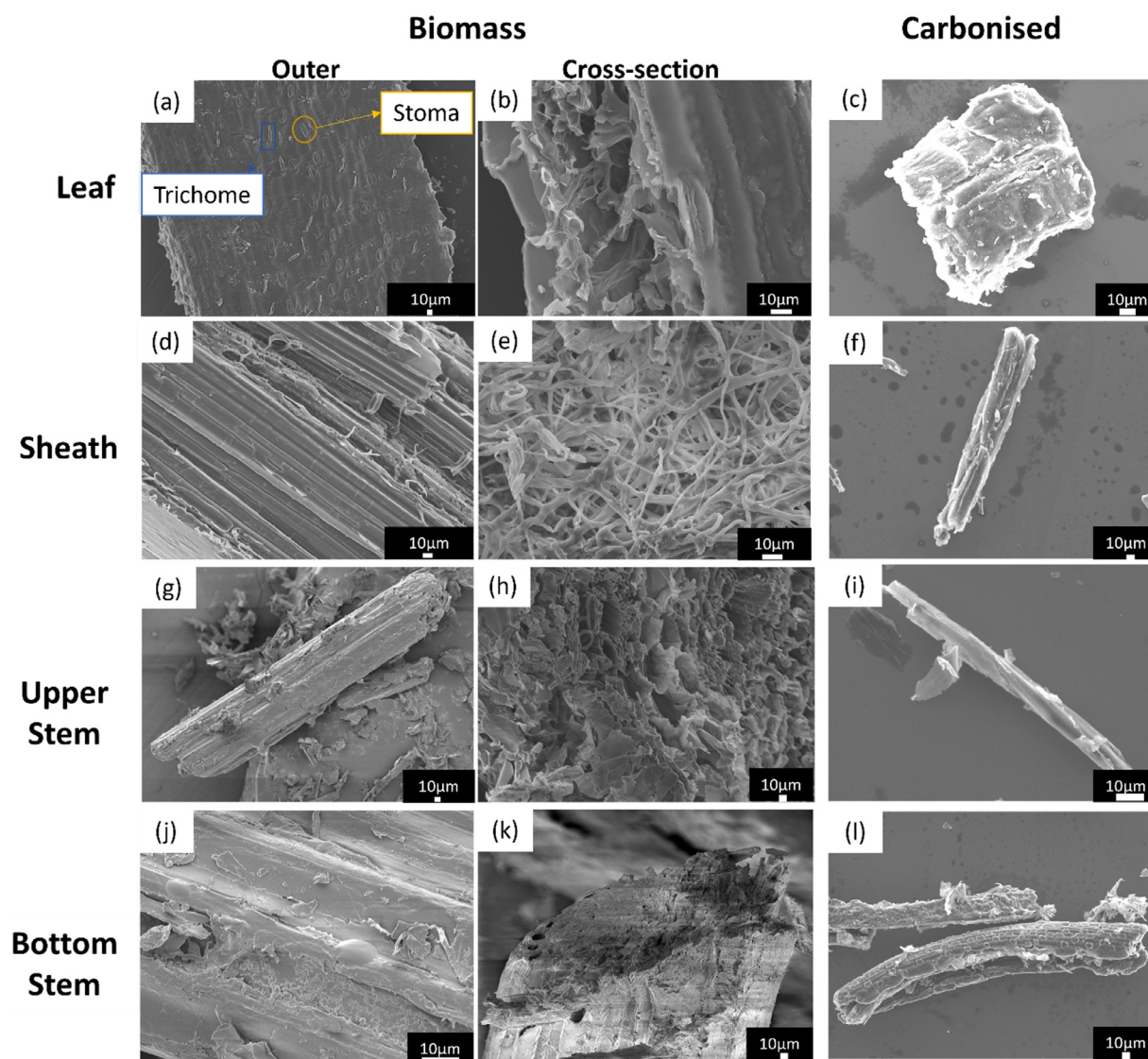
Fig. 4. SEM images of water-washed sorghum plant sections (leaf, sheath, upper stem and bottom stem) before and after carbonisation.

reveals many sheet-like structures and cavities (particularly void spaces). These cavities are more open and elongated. (Fig. 4b). The sheath surface (Fig. 4d) is clean and comprises smooth linear arrangements of fibres, while the cross-section (Fig. 4e) shows long agglomerated thread-like structures with small void spaces. The stem shows dense structures with minute pores. The surface morphology of the upper stem shows a smooth surface, but with obvious underlying anisotropy and orientation in the stem direction binding microfibres together into a bundle (Fig. 4g).

The upper stem cross-section SEM image reveals the presence of sheet-like structures. Additionally, duct-like structures are observed, and these are conduits to transfer water and other required nutrients for plant growth (Fig. 4h) Fig. 4.j shows the outer surface of the bottom stem, which shows the rough surface with humps and cavities. SEM cross-sectional image of the bottom stem (Fig. 4k) shows long and thick fibres bundled together tightly. Energy-dispersive X-ray spectroscopy (EDX) measurements were performed for sorghum plant sections (Table 1). Elemental analysis indicates higher carbon wt.% content in the upper stem, while the sheath shows the higher oxygen amount. Additionally, elements other than carbon and oxygen also exist; for example, the leaf has

Si and Ca, the sheath has Si, the upper stem has K, and the bottom stem shows the existence of Si, Cl and K.

SEM images of carbon material derived from sorghum plant leaf, sheath, upper stem and bottom stem sections are presented in Fig. 4c, f, I and l, respectively. More rod-like structures were observed in the sorghum sheath, upper stem and bottom stem-derived carbons, while a higher percentage of sheet-like structures were observed in the sorghum leaf-derived carbon. In addition to the native plant cell wall architectures, this might be partly driven by a higher amount of lignin in the leaves. Upon pyrolysis, lignin tends to transform to nanosheets due to planar molecular architecture and the more robust thermal stability of these aromatic units. This 2d sheet-like structure is often accompanied by a high surface area [16]. Additionally, interesting spots on the carbonised bottom stem material are observed in the SEM image (Fig. 4l). These might be due to the presence of silica. As already mentioned in the XRD section, the high-intensity signatures in the XRD pattern of the bottom stem are due to these inorganic components. EDX was used for analysing the presence of inorganic components in carbonised samples. As represented in Table 2, the bottom stem showed a higher amount of carbon content after carbonisation,

while a higher presence of oxygen was noted in the sheath. In addition to carbon and oxygen, Si and other elements (Mg, P, Ca, K and Cl) were persistent across the upper and lower stem after carbonisation. Depending on the application requirements, these inorganic contaminants may be removed either at the stage of biorefining or after carbonisation.

X-ray photoelectron spectroscopy (XPS)

The X-ray photoelectron spectroscopy (XPS) survey scan for all sorghum sections is presented in Figure S1 (Supplementary material). The accompanying percentage of carbon and oxygen is presented in Table 1. It is noted from the C 1 s high-resolution XPS spectra that carbon and oxygen are the main surface elements present, with traces of nitrogen, silicon and strontium. The high-resolution carbon spectra Fig. 5 (a-d) of biomass sorghum were deconvoluted into C−C, C−O-C, C = O, and COOH [28, 57]. The intensity of C−O-C, associated with pure cellulose and C−C, is associated with aliphatic and aromatic carbon backbones [37]. The leaf presents the highest C−C intensity, consistent with the lignocellulosic composition results. On the other hand, the stems show the highest intensity for C−O-C, showing cellulose is the main surface element for stem sections.

The X-ray photoelectron spectroscopic (XPS) survey of carbonised samples is presented in Figure S1 (Supplementary material). The accompanying percentage of carbon and oxygen is presented in Table 2. The C 1 s peak is at about 285 eV. The upper stem shows the highest percentage of carbon (92.0 at%), while the bottom stem, leaf and sheath show 91, 82 and 76 at%, respectively. Dopants such as oxygen have a high influence on the properties of carbon materials. The XPS survey shows O1s peak at about 534 eV (Figure S1, Supplementary material). The sheath has the highest levels of 18 at% oxygen, while leaf, bottom stem and upper stem show 14, 8 and 7 at%, respectively. The C 1 s spectrum of carbonised samples was deconvoluted (Fig. 5(e-h)) into a component of C−C/C = C (ca. 284 eV), C−O−C (ca. 286 eV) and C = O (ca. 287 eV). The spectra at ca. 290.0 eV are associated with $(\pi - \pi)$ graphitic carbons. It is noted that high $(\pi - \pi)$ graphitic carbons were produced in the presence of higher lignin and lower CrI values for the associated precursors. As mentioned earlier, this is most probably due to the higher thermal stability of aromatic units in lignin [16].

Nitrogen adsorption

The resulting carbonised sorghum plant sections were characterised by N_2 adsorption-desorption measurements. The pore size distribution curves (Fig. 6(a)) and the surface areas were calculated by the BJH and BET methods. All carbonised plant sections show the mixed Type I/IV isotherms, indicating the presence of a hierarchical distribution of micropores and mesopores. The initial uptake of N_2 at a low-pressure range ($P/P^0 < 0.1$) of the carbonised leaf is much larger compared to the sheath, upper stem and bottom stem (Fig. 6(b)). It is indicated that the carbonised leaf has a large number of micropores. The surface area derived from the micropores increases in the order of leaf > sheath > bottom stem > upper stem. This trend is associated with the lignin and ash content in the biomass precursor. Gergova et al. reported that lignin-derived char shows higher BET surface area (S_{BET}) and more total pore volume than char derived from cellulose [16,36,60]. In other reports, ash also shows association with carbon material porosity [43,44,61 63]. Similar trends are observed in this work, where the higher lignin and ash content plant sections (leaf > sheath > bottom stem > upper stem) have higher S_{BET} and pore volume (Figure S2 (Supplementary material)). ~~All carbonised plant sections show the mixed Type I/IV isotherms,~~

~~indicating the presence of a hierarchical distribution of micropores and mesopores.~~ The BET surface area for carbonised leaf, sheath, bottom stem and upper stem sections was 311, 197, 71 and 54 $m^2 \ g^{-1}$, respectively (Table 2). The larger BET surface area of carbonised leaf might be associated with large pore volume (Table 2), and potentially also due to the sheet-like morphological structure ~~, which was generated due to the influence of higher lignin content in the leaf~~ [16]. Thus, significant differences between carbonised sorghum plant sections are observed.

Thermal properties

Thermogravimetric analysis (TGA) is useful to investigate the thermal decomposition behaviour of lignocellulose precursors Fig. 7.(a) shows the TGA (weight loss curve), and Fig. 7(b) shows the derivative thermogravimetric (DTG) for water-washed sorghum plant sections. There is a notable difference in the carbonisation behaviour amongst the four plant sections. The initial weight loss range around ∼ 40 °C to 150 °C is related to the evaporation and desorption of fibre-bound water [37]. After dehydration, a complex process begins in which the decomposition of carbohydrates and lignin happens [31]. The onset decomposition temperature (T_o) is unique for every plant section. Higher T_o is associated with a higher thermal stability of biomass precursors. The Upper and bottom stem has the lowest T_o. The low thermal stability of stems is associated with a high content of extractives because extractives have lower molecular weight and high volatility. Hemicellulose decompositions start in the next temperature range and are associated with the weight losses observed between 220 °C to 315 °C. The sheath has a lower T_o compared to leaf, which might be due to the decomposition of high amounts of hemicellulose in the sheath. Hemicellulose has low thermal stability due to its amorphous structure and relatively low degree of polymerization. The cellulose phase decomposition range is between 315 °C to 400 °C [64]. Usually, all cellulose is carbonised when the temperature exceeds 400 °C. The bottom stem shows higher thermal stability when compared to the upper stem. This is interesting because although they have an almost identical morphology and lignocellulosic composition, they display significant differences in CrI. It is already reported that a higher degree of crystallinity and a higher amount of lignin can enhance the lignocellulose thermal stability [31,37,38]. Consequently, a higher temperature and energy are required for degradation.

Thermally stable lignin does not decompose easily. Usually, its decomposition occurs gradually over a wide temperature range, starting from ∼200 °C up to 700 °C. Additionally, lignin generally generates the highest solid residue [64]. The residual masses for leaf, sheath, upper and bottom stem were found from TGA at 500 °C to be 25.6, 24.9, 25 and 30 wt%, respectively. On the other hand, the manual calculation of percentage yield obtained after carbonisation at 1000 °C were 23, 26, 24 and 28 wt% for leaf, sheath, upper stem and bottom stem, respectively. These results show that all components contribute to the yield of activated products [16]. This difference in the calculations is because of two main factors. The first is temperature, and the other is the stabilisation step (which is missing in TGA). Hence, the lignocellulosic composition significantly influences the carbonisation behaviour, and this difference is due to the unique inherent structures and chemical natures of lignocellulosic components.

The Attenuated total reflectance Fourier transform infrared spectroscopy (ATR-FTIR) spectra of water-washed sorghum plant sections show a clear difference in the lignocellulosic chemical compositions between sorghum leaf, sheath and stems (Figure S3 (a)). The lower intensities for upper and bottom stems at 2920 cm^{-1} (Symmetrical C−H bond stretching in aromatic methoxyl, methyl and methylene groups, $C-H_2$ asymmetric stretching) [65],
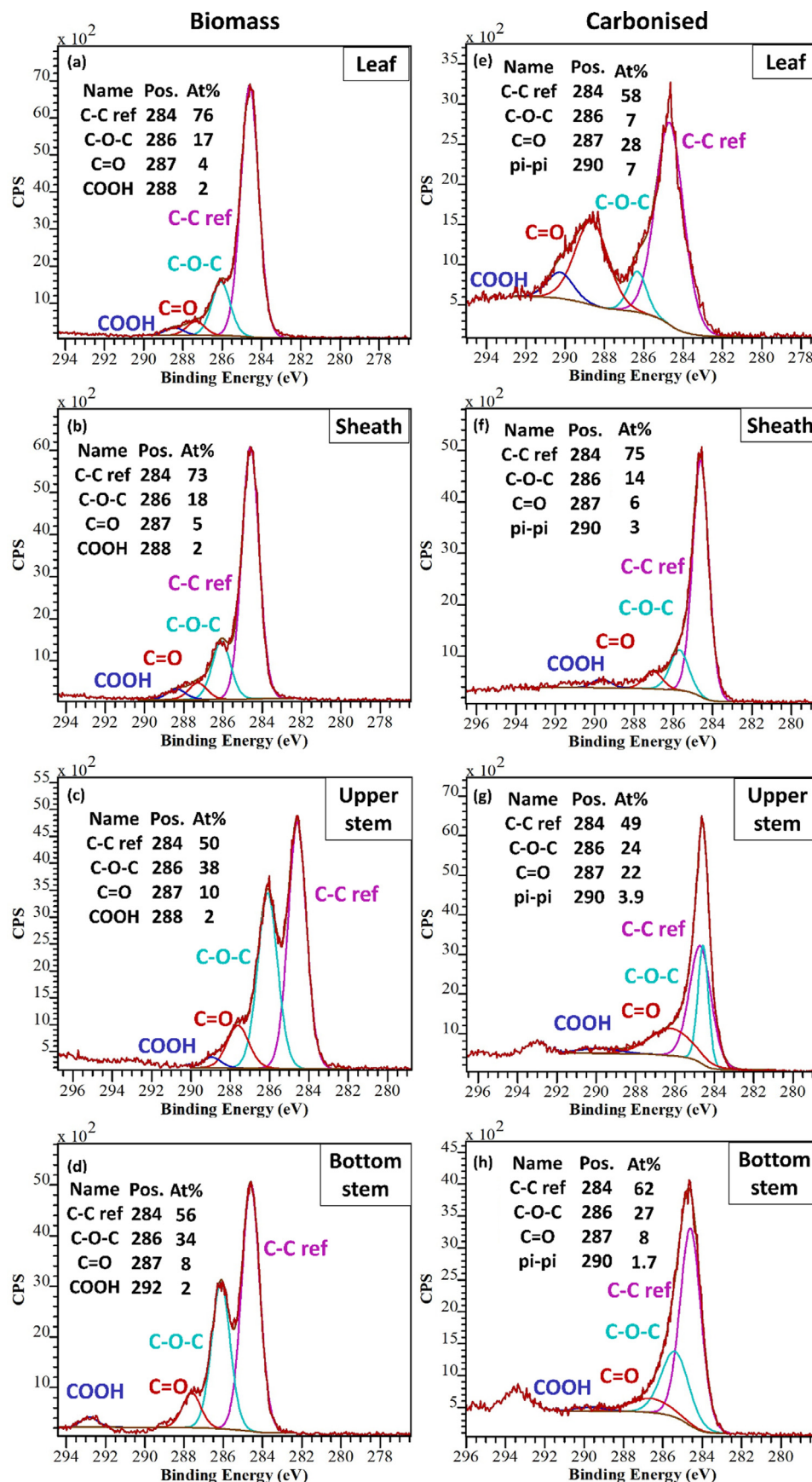
Fig. 5. High-resolution of carbon X-ray photoelectron spectroscopy (XPS) spectra for sorghum plant sections and associated derived carbons.
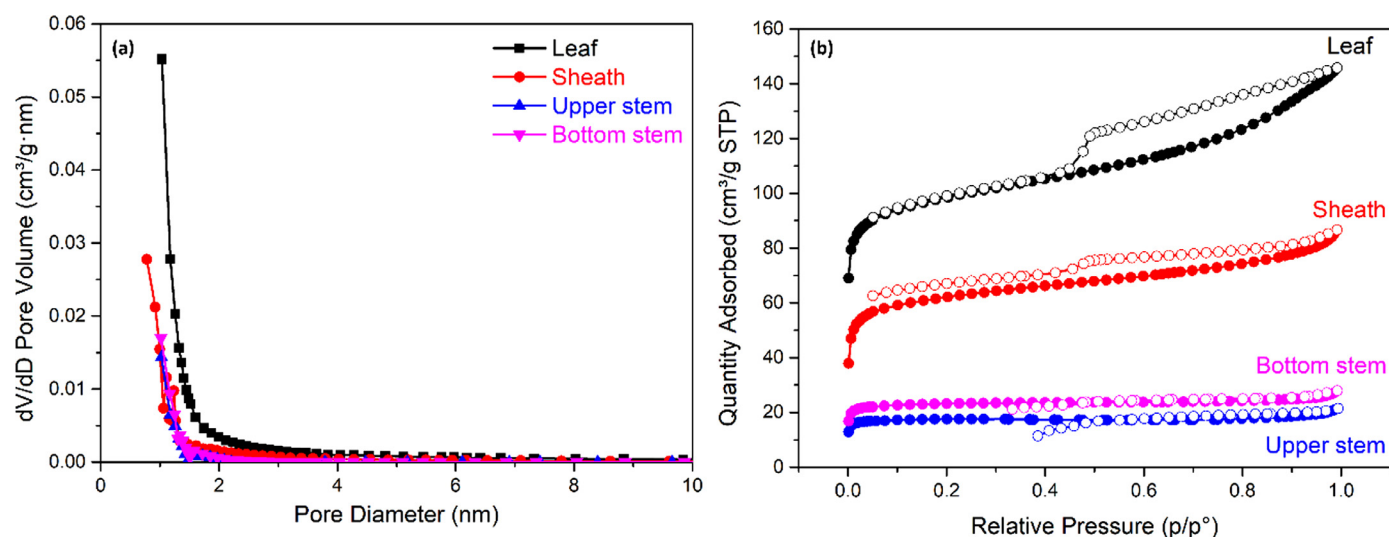
Fig. 6. Influence of morphology and lignocellulosic composition of different plant sections on the (a) Pore size distribution and (b) N_2 adsorption/desorption isotherm of carbonised samples.
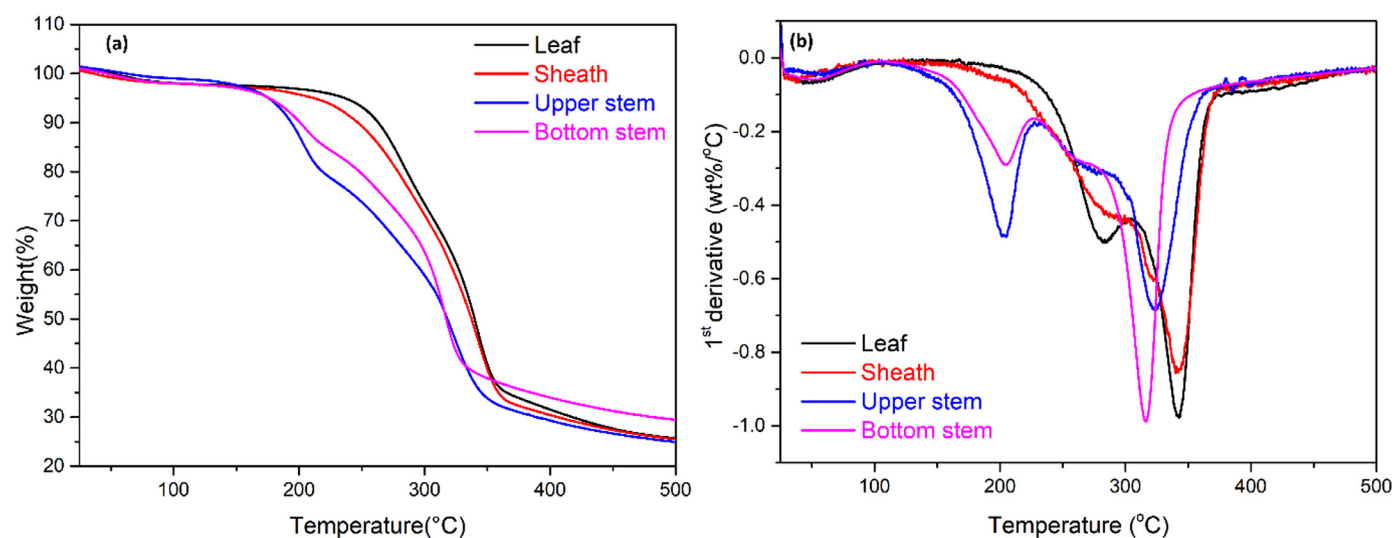
Fig. 7. (a) TGA and (b) DTG thermograms for water-washed sorghum plant sections under nitrogen flow.

and 2846 cm^{-1} (C–H stretching bond of alkane group) [37] and 817 cm^{-1} (C–H out of plane bending) [66] are associated with plant sections having lower lignin and hemicellulose contents, as compared to other sections of sorghum plants, i.e., leaf and sheath. These results are also in agreement with the results obtained through composition analysis presented in Table 1. After carbonisation (Figure S3 (b)), the peaks for the above discussed functional groups were disappeared. The presence of peaks in leaf and sheath carbon FTIR spectra can relate to the oxygen functional group. This can be associated with XPS results, which show high oxygen content in leaf and sheath.

Conclusions

This study investigates for the first time the variability in carbonisation behaviour of sorghum biomass as a function of different plant sections. We do this to arrive at a more sophisticated understanding of the relationship between lignocellulosic composition and the structure and properties of derived carbon materials. Sorghum (Sugargraze™) biomass was partitioned into four different plant sections: leaf, sheath, upper stem and bottom stem,

which exhibited differences in lignocellulosic composition, native plant cell wall hierarchical morphology, and crystallinity. Different plant sections generated unique carbon features (structure, morphology, porosity and yield) under identical pyrolysis conditions. The leaf with the highest lignin content yields 23% carbon with high crystallinity and the highest number of graphitic layers. This leaf section also exhibits high BET surface area and microporosity with sheet-like morphology. The sheath section with high cellulose content yields 26% carbon with thinner graphitic layers and a larger D-spacing compared to other sections. Stems with high extractives facilitate early-stage stabilisation. The upper stem yields 25% carbon and is accompanied by a low BET surface area and pore volume, whereas the bottom stem yields 30% carbon with a higher proportion of disordered carbon and a lower D-spacing. It is noted that the A_D/A_G ratio, an important measure of carbon quality for many applications, is correlated with an increase in the CrI and a decrease in the lignin content of the biomass precursor. Lignin and ash content in the precursor has a positive relationship with S_{BET} and the pore volume of the resulting carbon. Hence, carbon structure and properties can be judiciously controlled by selecting or blending different plant sections. For the future, this investiga-

tion of carbonisation behaviour also facilitates the development of a more sophisticated structure-property relationship for biomass-derived carbon materials.

Declaration of Competing Interest

The authors declare that they have no known competing financial interests or personal relationships that could have appeared to influence the work reported in this paper.

Acknowledgements

Supplementary materials

Supplementary material associated with this article can be found, in the online version, at doi:10.1016/j.cartre.2022.100168.

References

[1] P. Kalyani, A. Anitha, Biomass carbon & its prospects in electrochemical energy systems, Int. J. Hydrogen Energy 38 (2013) 4034–4045, doi:10.1016/j.ijhydene.2013.01.048.

[2] J. Wang, P. Nie, B. Ding, S. Dong, X. Hao, H. Dou, X. Zhang, Biomass derived carbon for energy storage devices, J. Mater. Chem. A 5 (2017) 2411–2428, doi:10.1039/C6TA08742F.

[3] H. Lu, X.S. Zhao, Biomass-derived carbon electrode materials for supercapacitors, Sustain. Energy Fuels 1 (2017) 1265–1281, doi:10.1039/C7SE00099E.

[4] Z. Gao, Y. Zhang, N. Song, X. Li, Biomass-derived renewable carbon materials for electrochemical energy storage, Mater. Res. Lett. 5 (2017) 69–88, doi:10.1080/21663831.2016.1250834.

[5] Q. Ma, Y. Yu, M. Sindoro, A.G. Fane, R. Wang, H. Zhang, Carbon-based functional materials derived from waste for water remediation and energy storage, Adv. Mater. 29 (2017) 1605361, doi:10.1002/adma.201605361.

[6] A.E.D. Mahmoud, Eco-friendly reduction of graphene oxide via agricultural byproducts or aquatic macrophytes, Mater. Chem. Phys. 253 (2020) 123336, doi:10.1016/j.matchemphys.2020.123336.

[7] A.E.D. Mahmoud, M. Franke, M. Stelter, P. Braeutigam, Mechanochemical versus chemical routes for graphitic precursors and their performance in micropollutants removal in water, Powder Technol. 366 (2020) 629–640, doi:10.1016/j.powtec.2020.02.073.

[8] S. Boufi, 6 - Agricultural crop residue as a source for the production of cellulose nanofibrils, in: M. Jawaid, S. Boufi, H.P.S A.K. (Eds.), Cellulose-Reinforced Nanofibre Composites, Woodhead Publishing, 2017, pp. 129–152.

[9] A.E.D. Mahmoud, m. Fawzy, A. Radwan, Optimization of Cadmium (CD2+) removal from aqueous solutions by novel biosorbent, Int. J. Phytoremediation 18 (2016) 619–625 https://doi:10.1080/15226514.2015.1086305.

[10] J. Pennells, I.D. Godwin, N. Amirialian, D.J. Martin, Trends in the production of cellulose nanofibers from non-wood sources, Cellulose 27 (2020) 575–593, doi:10.1007/s10570-019-02828-9.

[11] B.O. Abo, M. Gao, Y. Wang, C. Wu, H. Ma, Q. Wang, Lignocellulosic biomass for bioethanol: an overview on pretreatment, hydrolysis and fermentation processes, Rev. Environ. Health 34 (2019) 57–68 https://doi:10.1515/reveh-2018-0054.

[12] D.M. Alonso, S.H. Hakim, S. Zhou, W. Won, O. Hosseinaei, J. Tao, V. Garcia-Negron, A.H. Motagamwala, M.A. Mellmer, K. Huang, C.J. Houtman, N. Labbé, D.P. Harper, C.T. Maravelias, T. Runge, J.A. Dumesic, Increasing the revenue from lignocellulosic biomass: maximizing feedstock utilization, Sci. Adv. 3 (2017) e1603301, doi:10.1126/sciadv.1603301.

[13] A.E.D. Mahmoud, M. Fawzy, Chapter 7 - bio-based methods for wastewater treatment: green sorbents, in: G.S. Ansari A, R. Gill, G. Lanza, L. Newman (Eds.), Phytoremediation, Springer, Phytoremediation, 2016, pp. 209–238.

[14] P. González-García, Activated carbon from lignocellulosics precursors: a review of the synthesis methods, characterization techniques and applications, Renew. Sust. Energ. Rev. 82 (2018) 1393–1414, doi:10.1016/j.rser.2017.04.117.

[15] J. Górka, C. Vix-Guterl, C.Matei Ghimbeu, Recent progress in design of biomass-derived hard carbons for sodium ion batteries, C 2 (2016) 24. 10.3390/c2040024.

[16] J. Deng, T. Xiong, H. Wang, A. Zheng, Y. Wang, Effects of cellulose, hemicellulose, and lignin on the structure and morphology of porous carbons, ACS Sustain. Chem. Eng. 4 (2016) 3750–3756, doi:10.1021/acssuschemeng.6b00388.

[17] N. Reddy, Y. Yang, Structure and properties of natural cellulose fibers obtained from sorghum leaves and stems, J. Agric. Food Chem. 55 (2007) 5569–5574, doi:10.1021/jf0707379.

[18] B.T.S. Ramanujam, A.K. Nanjundan, P.K. Annamalai, Chapter 12 - Nanocellulose-based carbon as electrode materials for sodium-ion batteries, in: S. Thomas, Y.B. Pottathara (Eds.), Nanocellulose Based Composites For Electronics, Elsevier, 2021, pp. 295–312.

[19] M. Li, G. Yan, A. Bhalla, L. Maldonado-Pereira, P.R. Russell, S.-.Y. Ding, J.E. Mullet, D.B. Hodge, Physical fractionation of sweet sorghum and forage/energy sorghum for optimal processing in a biorefinery, Ind. Crops Prod. 124 (2018) 607–616, doi:10.1016/j.indcrop.2018.07.002.

[20] R.R. Gaddam, E. Jiang, N. Amirialian, P.K. Annamalai, D.J. Martin, N.A. Kumar, X.S. Zhao, Spinifex nanocellulose derived hard carbon anodes for high-performance sodium-ion batteries, Sustain. Energy Fuels 1 (2017) 1090–1097, doi:10.1039/C7SE00169J.

[21] B. Bakeer, I. Taha, H. El-Mously, S.A. Shehata, On the characterisation of structure and properties of sorghum stalks, Ain Shams Eng. J. 4 (2013) 265–271, doi:10.1016/j.asej.2012.08.001.

[22] J. Pennells, A. Cruickshank, C. Chaléat, I.D. Godwin, D.J. Martin, Sorghum as a novel biomass for the sustainable production of cellulose nanofibers, Ind. Crops Prod. 171 (2021) 113917, doi:10.1016/j.indcrop.2021.113917.

[23] J.M. Awika, in: Major Cereal Grains Production and Use around the World, Advances in Cereal Science: Implications to Food Processing and Health Promotion, American Chemical Society, 2011, pp. 1–13.

[24] A. Borrell, E. van Oosterom, B. George-Jaeggli, D. Rodriguez, J. Eyre, D.J. Jordan, E. Mace, V. Singh, V. Vadez, M. Bell, I. Godwin, A. Cruickshank, Y. Tao, G. Hammer, Chapter 5 - Sorghum, in: V.O. Sadras, D.F. Calderini (Eds.), Crop Physiology Case Histories for Major Crops, Academic Press, 2021, pp. 196–221.

[25] J.H. Houx III, C.A. Roberts, F.B. Fritschi, Evaluation of sweet sorghum bagasse as an alternative livestock feed, Crop Sci. 53 (2013) 1784–1790, doi:10.2135/cropsci2012.03.0190.

[26] S. Mathur, A.V. Umakanth, V.A. Tonapi, R. Sharma, M.K. Sharma, Sweet sorghum as biofuel feedstock: recent advances and available resources, Biotechnol. Biofuels 10 (2017) 146, doi:10.1186/s13068-017-0834-9.

[27] X. Zhu, X. Jiang, X. Liu, L. Xiao, Y. Cao, A green route to synthesize low-cost and high-performance hard carbon as promising sodium-ion battery anodes from sorghum stalk waste, Green Energy Environ. 2 (2017) 310–315, doi:10.1016/j.gee.2017.05.004.

[28] M. Kim, H. Lim, X. Xu, M.S.A. Hossain, J. Na, N.N. Awaludin, J. Shah, L.K. Shrestha, K. Ariga, A.K. Nanjundan, D.J. Martin, J.G. Shapter, Y. Yamauchi, Sorghum biomass-derived porous carbon electrodes for capacitive deionization and energy storage, Microporous Mesoporous Mater. 312 (2021) 110757, doi:10.1016/j.micromeso.2020.110757.

[29] J. Pennells, B. Heuberger, C. Chaléat, D.J. Martin, Assessing cellulose micro/nanofibre morphology using a high throughput fibre analysis device to predict nanopaper performance, Cellulose (2022) https://10.1007/s10570-021-04405-5.

[30] L. Segal, J.J. Creely, A.E. Martin, C.M. Conrad, An empirical method for estimating the degree of crystallinity of native cellulose using the x-ray diffractometer, Text. Res. J. 29 (1959) 786–794, doi:10.1177/004051755902901003.

[31] Y. Meng, C.I. Contescu, P. Liu, S. Wang, S.-.H. Lee, J. Guo, T.M. Young, Understanding the local structure of disordered carbons from cellulose and lignin, Wood Sci. Technol. 55 (2021) 587–606, doi:10.1007/s00226-021-01286-6.

[32] J. Wang, L. Yan, Q. Ren, L. Fan, F. Zhang, Z. Shi, Facile hydrothermal treatment route of reed straw-derived hard carbon for high performance sodium ion battery, Electrochim. Acta 291 (2018) 188–196, doi:10.1016/j.electacta.2018.08.136.

[33] A. Zoghlami, G. Paës, Lignocellulosic biomass: understanding recalcitrance and predicting hydrolysis, Front. Chem. 7 (2019) doi:10.3389/fchem.2019.00874.

[34] N. Reddy, Y. Yang, Biofibers from agricultural byproducts for industrial applications, Trends Biotechnol. 23 (2005) 22–27, doi:10.1016/j.tibtech.2004.11.002.

[35] Q. Liu, L. Luo, L. Zheng, Lignins: biosynthesis and biological functions in plants, Int. J. Mol. Sci. 19 (2018) 335, doi:10.3390/ijms19020335.

[36] Y. Xue, C. Du, Z. Wu, L. Zhang, Relationship of cellulose and lignin contents in biomass to the structure and RB-19 adsorption behavior of activated carbon, New J. Chem. 42 (2018) 16493–16502 https://10.1039/C8NJ03007C.

[37] A. Hosseinmardi, P.K. Annamalai, B. Martine, J. Pennells, D.J. Martin, N. Amirialian, Facile tuning of the surface energy of cellulose nanofibers for nanocomposite reinforcement, ACS Omega 3 (2018) 15933–15942, doi:10.1021/acsomega.8b02104.

[38] S. E D. Chen, D. Gao, S.C. Capareda, F. Jia, Y. Wang, Influences of hydrochloric acid washing on the thermal decomposition behavior and thermodynamic parameters of sweet sorghum stalk, Renew. Energ. 148 (2020) 1244–1255, doi:10.1016/j.renene.2019.10.064.

[39] M.M. Tang, R. Bacon, Carbonization of cellulose fibers—I. Low temperature pyrolysis, Carbon 2 (1964) 211–220, doi:10.1016/0008-6223(64)90035-1.

[40] J. Batog, J. Frankowski, A. Wawro, A. Łacka, Bioethanol production from biomass of selected sorghum varieties cultivated as main and second crop, Energies 13 (2020) 6291, doi:10.3390/en13236291.

[41] J. Baruah, B.K. Nath, R. Sharma, S. Kumar, R.C. Deka, D.C. Baruah, E. Kalita, Recent Trends in the pretreatment of lignocellulosic biomass for value-added products, Front. Energy Res. 6 (2018) https://10.3389/fenrg.2018.00141.

[42] L. Leng, Q. Xiong, L. Yang, H. Li, Y. Zhou, W. Zhang, S. Jiang, H. Li, H. Huang, An overview on engineering the surface area and porosity of biochar, Sci. Total Environ. 763 (2021) 144204, doi:10.1016/j.scitotenv.2020.144204.

[43] Y. Zhu, Z. Li, J. Chen, Applications of lignin-derived catalysts for green synthesis, Green Energy Environ. 4 (2019) 210–244, doi:10.1016/j.gee.2019.01.003.

[44] W.N.R.W. Isahak, M.W.M. Hisham, M.A. Yarmo, Highly Porous Carbon Materials from Biomass by Chemical and Carbonization Method: a Comparison Study, J. Chem. 2013 (2013) 620346, doi:10.1155/2013/620346.

[45] Y. Okahisa, K. Abe, M. Nogi, A.N. Nakagaito, T. Nakatani, H. Yano, Effects of delignification in the production of plant-based cellulose nanofibers for optically transparent nanocomposites, Compos. Sci. Technol. 71 (2011) 1342–1347, doi:10.1016/j.compscitech.2011.05.006.

[46] S.-.H. Lee, F. Chang, S. Inoue, T. Endo, Increase in enzyme accessibility by generation of nanospace in cell wall supramolecular structure, Bioresour. Technol. 101 (2010) 7218–7223, doi:10.1016/j.biortech.2010.04.069.

[47] M. Delgado-Aguilar, I. González, Q. Tarrés, M.À. Pèlach, M. Alcalà, P. Mutjé, The key role of lignin in the production of low-cost lignocellulosic nanofibres for papermaking applications, Ind. Crops Prod. 86 (2016) 295–300, doi:10.1016/j.indcrop.2016.04.010.

[48] C.-.W. Park, S.-.Y. Han, H.-.W. Namgung, P.-n. Seo, S.-.Y. Lee, S.-.H. Lee, Preparation and characterization of cellulose nanofibers with varying chemical compositions, Bioresources 12 (2017) 14, doi:10.15376/biores.12.3.5031-5044.

[49] A. Balea, N. Merayo, E. De La Fuente, C. Negro, Á. Blanco, Assessing the influence of refining, bleaching and TEMPO-mediated oxidation on the production of more sustainable cellulose nanofibers and their application as paper additives, Ind. Crops Prod. 97 (2017) 374–387, doi:10.1016/j.indcrop.2016.12.050.

[50] S. Iwamoto, K. Abe, H. Yano, The effect of hemicelluloses on wood pulp nanofibrillation and nanofiber network characteristics, Biomacromolecules 9 (2008) 1022–1026, doi:10.1021/bm701157n.

[51] A. Chaker, S. Alila, P. Mutjé, M.R. Vilar, S. Boufi, Key role of the hemicellulose content and the cell morphology on the nanofibrillation effectiveness of cellulose pulps, Cellulose 20 (2013) 2863–2875, doi:10.1007/s10570-013-0036-y.

[52] J.P. Vandenbrink, R.N. Hilten, K.C. Das, A.H. Paterson, F.A. Feltus, Analysis of crystallinity index and hydrolysis rates in the bioenergy crop sorghum bicolor, Bioenergy Res. 5 (2012) 387–397, doi:10.1007/s12155-011-9146-2.

[53] A.K. Nanjundan, R.R. Gaddam, A.H. Farokh Niaei, P.K. Annamalai, D.P. Dubal, D.J. Martin, Y. Yamauchi, D.J. Searles, X.S. Zhao, Potassium-ion storage in cellulose-derived hard carbon: the role of functional groups, Batter. Supercaps 3 (2020) 953–960, doi:10.1002/batt.202000116.

[54] A.M. Dehkhoda, N. Ellis, E. Gyenge, Electrosorption on activated biochar: effect of thermo-chemical activation treatment on the electric double layer capacitance, J. Appl. Electrochem. 44 (2014) 141–157, doi:10.1007/s10800-013-0616-4.

[55] F. Attia, L. Martinez, T. Lamaze, Foliar application of processed calcite particles improves leaf photosynthesis of potted Vitis vinifera L. (var. 'Cot') grown under water deficit, J. Int. Sci. Vigne Vin 48 (2014) 237–245, doi:10.20870/oeno-one.2014.48.4.1691.

[56] Y.E. Kim, S.J. Yeom, J.-.E. Lee, S. Kang, H. Kang, G.-.H. Lee, M.J. Kim, S.G. Lee, H.-.W. Lee, H.G. Chae, Structure-dependent sodium ion storage mechanism of cellulose nanocrystal-based carbon anodes for highly efficient and stable batteries, J. Power Sources 468 (2020) 228371, doi:10.1016/j.jpowsour.2020.228371.

[57] X. Xu, Y. Cui, J. Shi, W. Liu, S. Chen, X. Wang, H. Wang, Sorghum core-derived carbon sheets as electrodes for a lithium-ion capacitor, RSC Adv. 7 (2017) 17178–17183, doi:10.1039/C7RA02279D.

[58] F.S. da Luz, F.d.C. Garcia Filho, M.T.G. del-Río, L.F.C. Nascimento, W.A. Pinheiro, S.N. Monteiro, Graphene-incorporated natural fiber polymer composites: a first overview, Polymers 12 (2020) 1601, doi:10.3390/polym12071601.

[59] T. Ichie, Y. Inoue, N. Takahashi, K. Kamiya, T. Kenzo, Ecological distribution of leaf stomata and trichomes among tree species in a Malaysian lowland tropical rain forest, J. Plant Res. 129 (2016) 625–635, doi:10.1007/s10265-016-0795-2.

[60] S. Chatterjee, T. Saito, Lignin-derived advanced carbon materials, ChemSusChem 8 (2015) 3941–3958, doi:10.1002/cssc.201500692.

[61] M. Biswal, A. Banerjee, M. Deo, S. Ogale, From dead leaves to high energy density supercapacitors, Energy Environ. Sci. 6 (2013) 1249–1259 https://10.1039/C3EE22325F.

[62] M. Sevilla, A.B. Fuertes, A general and facile synthesis strategy towards highly porous carbons: carbonization of organic salts, J. Mater. Chem. A. 1 (2013) 13738–13741 https://10.1039/C3TA13149A.

[63] J. Li, Y. Gao, K. Han, J. Qi, M. Li, Z. Teng, High performance hierarchical porous carbon derived from distinctive plant tissue for supercapacitor, Sci. Rep. 9 (2019) 17270 https://10.1038/s41598-019-53869-w.

[64] H. Yang, R. Yan, H. Chen, D.H. Lee, C. Zheng, Characteristics of hemicellulose, cellulose and lignin pyrolysis, Fuel 86 (2007) 1781–1788, doi:10.1016/j.fuel.2006.12.013.

[65] A. Hosseinmardi, P.K. Annamalai, L. Wang, D. Martin, N. Amiralian, Reinforcement of natural rubber latex using lignocellulosic nanofibers isolated from spinifex grass, Nanoscale 9 (2017) 9510–9519, doi:10.1039/C7NR02632C.

[66] Y. Horikawa, S. Hirano, A. Mihashi, Y. Kobayashi, S. Zhai, J. Sugiyama, Prediction of lignin contents from infrared spectroscopy: chemical digestion and lignin/biomass ratios of cryptomeria japonica, Appl. Biochem. Biotechnol. 188 (2019) 1066–1076, doi:10.1007/s12010-019-02965-8.